

A NEW SATELLITE-BASED METHODOLOGY FOR CONTINENTAL-SCALE DISTURBANCE DETECTION

DAVID J. MILDREXLER,¹ MAOSHENG ZHAO, FAITH ANN HEINSCH, AND STEVEN W. RUNNING

Numerical Terradynamic Simulation Group, Department of Ecosystem and Conservation Sciences, University of Montana, Missoula, Montana 59812 USA

Abstract. The timing, location, and magnitude of major disturbance events are currently major uncertainties in the global carbon cycle. Accurate information on the location, spatial extent, and duration of disturbance at the continental scale is needed to evaluate the ecosystem impacts of land cover changes due to wildfire, insect epidemics, flooding, climate change, and human-triggered land use. This paper describes an algorithm developed to serve as an automated, economical, systematic disturbance detection index for global application using Moderate Resolution Imaging Spectroradiometer (MODIS)/Aqua Land Surface Temperature (LST) and Terra/MODIS Enhanced Vegetation Index (EVI) data from 2003 to 2004. The algorithm is based on the consistent radiometric relationship between LST and EVI computed on a pixel-by-pixel basis. We used annual maximum composite LST data to detect fundamental changes in land-surface energy partitioning, while avoiding the high natural variability associated with tracking LST at daily, weekly, or seasonal time frames. Verification of potential disturbance events from our algorithm was carried out by demonstration of close association with independently confirmed, well-documented historical wildfire events throughout the study domain. We also examined the response of the disturbance index to irrigation by comparing a heavily irrigated poplar tree farm to the adjacent semiarid vegetation. Anomalous disturbance results were further examined by association with precipitation variability across areas of the study domain known for large interannual vegetation variability. The results illustrate that our algorithm is capable of detecting the location and spatial extent of wildfire with precision, is sensitive to the incremental process of recovery of disturbed landscapes, and shows strong sensitivity to irrigation. Disturbance detection in areas with high interannual variability of precipitation will benefit from a multiyear data set to better separate natural variability from true disturbance.

Key words: *disturbance recovery; ecosystem variability; landscape disturbance; MODIS/Aqua Land Surface Temperature; wildfire.*

INTRODUCTION

Landscape-level spatial data of disturbance location and intensity on the earth surface are important for tracking responses of the biosphere to climate change, for global carbon budget modeling, and for improved resource management. An ecological disturbance is an event that results in a sustained disruption of ecosystem structure and function (Pickett and White 1985, Tilman 1985). Similarly, we define disturbance as any factor that brings about a significant change in the ecosystem leaf area index (LAI) for a period of more than one year (Waring and Running 1998). Disturbance can have both negative (e.g., wildfire) and positive (e.g., irrigation) effects on the LAI and may occur naturally (e.g., wildfires, storms, or floods) or may be human induced, such as clearing for agriculture, clear-cutting in forests, building roads, altering stream channels, or irrigating land (Dale et al. 2000). The effects of disturbances are

controlled in large part by their intensity, duration, frequency, timing, and spatial impact (i.e., the size and shape of the area affected; Sousa 1984, Pickett and White 1985, Pickett et al. 1987, Reice 1994, Turner et al. 1997). Disturbances may affect both above- and belowground processes (Dale et al. 2000), and many of these disturbance events alter ecosystem productivity and resource availability on large spatial and temporal scales (Potter et al. 2003). Ecosystem scientists have yet to develop a proven methodology to monitor and understand major disturbance events and their historical regimes at a global scale (Potter et al. 2003).

Because major “pulses” of CO₂ from the loss of terrestrial biomass are emitted to the atmosphere during large disturbance events, the timing, location, and magnitude of vegetation disturbance is presently a major uncertainty in understanding the global carbon cycle (Canadell et al. 2000). Elevated biogenic sources of CO₂ have global implications for climatic change, which can, in turn, affect a vast number of species on earth and the functioning of virtually all ecosystems (Potter et al. 2003). For example, van der Werf et al. (2004) estimated that the global carbon emissions anomaly ($\pm 95\%$ CI)

Manuscript received 23 September 2005; revised 24 April 2006; accepted 1 May 2006. Corresponding Editor: H. P. Schmid.

¹ E-mail: drexler@ntsg.umt.edu

from fires during the 1997–1998 El Niño was 2.1 ± 0.8 Pg of carbon. Amiro et al. (2001) estimated direct emissions of carbon from Canadian forest fires for all of Canada for the period from 1959 to 1999, with a mean annual estimate of 27 ± 6 Tg C/yr. While such estimates provide insight into the magnitude of the potential contribution of fire emissions to atmospheric carbon, more accurate information on disturbance location, area, intensity, and recovery will help reduce the level of uncertainty and, therefore, provide relatively accurate information on the contribution of wildfire to carbon fluxes. Conversely, irrigation can be considered a positive disturbance that increases the leaf area of the irrigated land area, changes the energy balance of the land surface, and can result in increased ecosystem carbon accumulation. In the United States, there were an estimated $223\,850$ km 2 of irrigated agricultural area in 2003 (Food and Agriculture Organization, *available online* [last updated January 2006]).² Carbon accumulation in ecosystems recovering from disturbance or undergoing intensive management, such as irrigated farm lands, are high compared with chronosequence studies that suggest much lower long-term values in natural landscapes (Schimel et al. 2001). Accurate information on changes in irrigated land area is important for understanding the contribution of these lands to carbon fluxes.

Leafy vegetation cover, such as is measured by spectral vegetation indices (VI), is likely the most fragile and, therefore, perhaps the single most vulnerable *biotic* component of terrestrial ecosystems to detectable alteration during disturbance events (Potter et al. 2003). Midday radiometric land surface temperature (LST) is strongly related to vegetation density and is, therefore, perhaps the single most vulnerable *abiotic* component of terrestrial ecosystems to detectable alteration during disturbance events. Disturbances such as drought, wildfire, insect defoliation, urban development, and irrigation result in conditions that alter vegetation and, therefore, the energy balance of a site. Coupling LST with the Enhanced Vegetation Index (EVI) from the Moderate Resolution Imaging Spectroradiometer (MODIS) is a logical and dynamic approach to measure both the energy exchange consequence and the vegetation density changes resulting from disturbance.

The coupling of LST and spectral VIs

Early applications of satellite-derived LST aimed to analyze the energy budget at the earth surface for relating evapotranspiration (ET) and soil moisture to surface temperature from a bare surface (Carlson et al. 1981, Sequin and Itier 1983, Gurney and Camillo 1984). Goward et al. (1985) suggest using the rate of change in LST with the amount of vegetation to describe surface

characteristics. The underlying principle for such a technique is that LST decreases with an increase in vegetation density through latent heat transfer.

Infrared remotely sensed LST was used in association with the Normalized Difference Vegetation Index (NDVI) as a measure of energy balance Bowen ratios to evaluate land surface resistance and evapotranspiration (Hope et al. 1986, Goward and Hope 1989, Nemani and Running 1989, Carlson et al. 1990, Nemani et al. 1993) and showed a strong negative relation between remotely sensed spectral vegetation indices (VIs) and surface temperature (Goward et al. 1985, Price 1990, Smith and Choudhury 1991, Friedl and Davis 1994, Nemani and Running 1997, Wan et al. 2004). Goetz (1997) reported that the negative correlation between LST and NDVI, observed at several scales (25 m 2 to 1.2 km 2), was largely due to changes in vegetation cover and soil moisture and indicated that the surface temperature can rise rapidly with water stress.

Many previous applications of coarse-scale remote sensing data for land cover mapping and land cover change analysis were based on multi-temporal NDVI data (Lambin and Ehrlich 1996). Running et al. (1994) suggested that the addition of LST to spectral VIs can increase the discrimination of regional land cover classes. Lambin and Ehrlich (1996) explored the biophysical justification for such a combination and concluded that the main reason to perform land cover mapping and land cover change analysis in the LST–NDVI space rather than in the more traditional red vs. near-infrared spectral space is because the former contains information on many more biophysical attributes and processes of land surfaces than the latter. In other words, it characterizes land surfaces more completely than vegetation cover only. The coupling of LST and NDVI was found to substantially improve land cover characterization for regional- and continental-scale land cover classification (Lambin and Ehrlich 1995, Nemani and Running 1997, Roy et al. 1997). As a metric for land cover change detection, LST/NDVI ratio metrics were statistically better at detecting changes than the NDVI metric, confirming the importance of LST data as a complementary source of information to NDVI data (Borak et al. 2000).

The conceptual diagram developed by Nemani and Running (1997) divides the LST–NDVI space into four simple groups chosen to represent common energy absorption and exchange characteristics of various land cover types (Fig. 1). When land covers are stratified within the LST–NDVI space, an energy exchange trajectory results, where decreasing vegetation density is coupled with increasing LST. Disturbance causes shifts in the LST–NDVI energy exchange relationship and movement along the disturbance trajectory.

These previous studies took a snapshot or used time series to track the seasonal trajectory of the LST–NDVI relationship. However, satellite-derived LST is influenced by synoptic weather variability (wind speed, cloud

² (<http://faostat.fao.org/>)

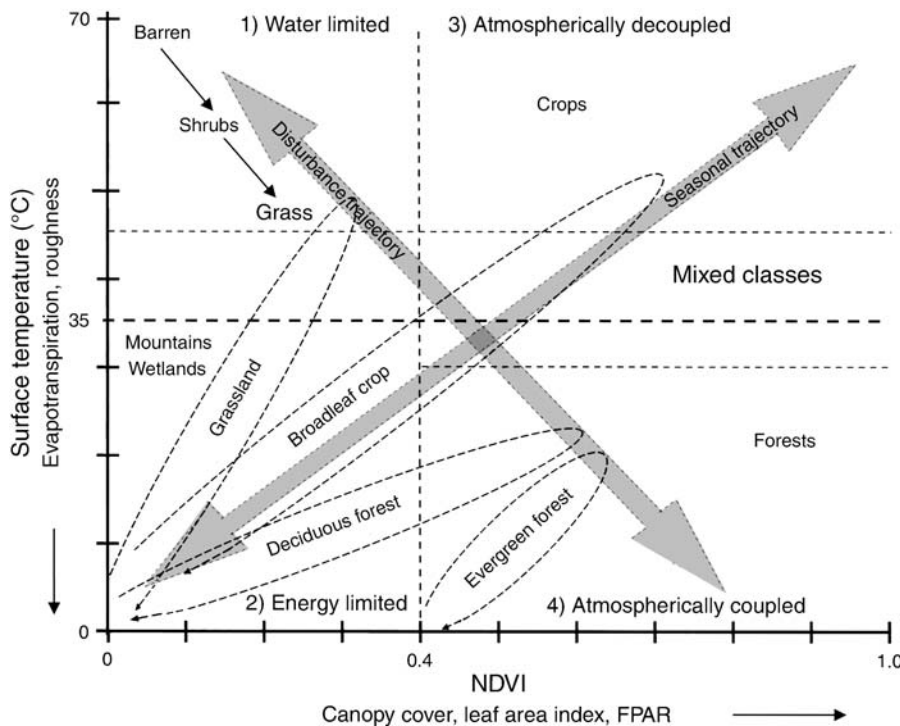


FIG. 1. Dynamics of surface temperature (T_s)-Normalized Difference Vegetation Index (NDVI) for various vegetation types where seasonal trajectories (dashed lines) indicate phenological evolution of vegetation, and the disturbance trajectory is useful for the detection of change over time. The disturbance trajectory arrow illustrates the negative relationship between the land surface temperature (LST) and NDVI and the potential for land cover shifts along the energy exchange trajectory as a result of disturbance (redrawn from Nemani and Running [1997]).

cover, humidity, radiation loading, etc.) on a daily, even hourly, basis, and has high natural variability (Friedl and Davis 1994, Nemani and Running 1997). Because our aim was to develop a simple, fast, automated disturbance detection algorithm for global application, we consciously chose annual maximum compositing of LST data in order to remove the information on surface dynamics related to synoptic weather conditions and seasonal patterns. By tracking the multiyear annual maximum composite LST, we focused on the land surface temperature under driest conditions. We used EVI because saturation levels are avoided, whereas NDVI tends to approach saturation level in high biomass regions, having important consequences for change detection (Huete et al. 2002).

Ecosystem disturbance theory

Disturbance by definition is an event that occurs outside the range of natural variability. Therefore, it is critical to clearly distinguish between disturbance and the backdrop of natural variability in the development of a disturbance index. Disturbance processes vary in their rate of departure from the range of natural variability. Instantaneous disturbances such as wildfire result in an immediate departure of the LST/EVI ratio from the range of natural variability, whereas non-instantaneous disturbances (e.g., drought, insect defoli-

ation) depart incrementally, or can return toward the range of natural variability after a brief departure, as in the case of short-term drought. Ideally, the range of natural variability is defined by assessing the interannual variability over a multiple-year data set.

Furthermore, land covers have unique ranges of natural variability. For example, patterns in interannual variability of annual net primary productivity (ANPP) for forested sites are distinctly less variable than in other biomes, whereas herbaceous plants in arid and semiarid ecosystems, such as the grasslands of the central United States, have the capacity for large and rapid production responses to unusually high or low precipitation levels (Knapp and Smith 2001, Holmgren et al. 2006). Because water-limited regions with relatively high production potential are very sensitive in net primary production (NPP) in response to variation in precipitation (Huxman et al. 2004), it is important to assess the interannual variability over multiple years when defining the range of natural variability for these ecosystems.

Based on two full years of Aqua and Terra/MODIS data, we present the initial development of an ongoing global disturbance monitoring algorithm that will, with each additional year, more accurately define the range of natural variability and redefine disturbance. Our objective was to create an automated system that uses annual maximum composite LST data to track both positive

and negative changes in land surface energy partitioning while avoiding the natural synoptic variability associated with daily to seasonal LST. We expect that disturbance resulting in decreased vegetation density should lead to an increase in LST as sensible heat flux increases. Conversely, disturbance resulting in increased vegetation density (irrigated farmland) should be coupled with decreasing LST.

METHODS

Disturbance index development

We developed a simple, yet powerful, algorithm to identify significant interannual changes in surface energy partitioning. As a result, we used the ratio of annual maximum composite LST and EVI in order to detect land surface disturbance, such that

$$\text{DI}_{\text{LST/EVI}} = \frac{\text{LST}_{\max}/\text{EVI}_{\max}}{\text{LST}_{\bar{X}\max}/\text{EVI}_{\bar{X}\max}} \quad (1)$$

where $\text{DI}_{\text{LST/EVI}}$ is the disturbance index (DI) value, LST_{\max} is the annual maximum eight-day composite LST, EVI_{\max} is the annual maximum 16-day EVI, $\text{LST}_{\bar{X}\max}$ is the multiyear mean of LST_{\max} , and $\text{EVI}_{\bar{X}\max}$ is the multiyear mean of EVI_{\max} . $\text{DI}_{\text{LST/EVI}}$ is a dimensionless value that, in the absence of disturbance, approaches unity.

First, we applied annual maximum value compositing to the data, selecting independently for each pixel the maximum eight-day LST and 16-day EVI over a one-year period. The LST_{\max} and EVI_{\max} values were each compiled into a separate GIS layer for each year. The LST_{\max} during a given year was divided by the EVI_{\max} value during the same year on a pixel-by-pixel basis, resulting in a ratio of LST_{\max} to EVI_{\max} . Prior to this division, a baseline boundary condition of 0.025 was established and all pixels with EVI values less than the boundary value were reclassified as no data in the 2003 and 2004 maximum EVI images. These values were primarily associated with water bodies and snow/ice, and the basic premise that the lower baseline contains only non-photosynthetic targets (Huete et al. 1999). EVI values in the lower baseline are problematic in the calculation of the DI because order-of-magnitude differences exist between maximum EVI values on an interannual basis for a given pixel within the baseline boundary condition, and EVI is in the denominator for the annual calculation (Eq. 1). Pixels that have good quality data for only one of the two years were classified as having "no data." The 2004 LST/EVI ratio was then divided by the 2003 LST/EVI ratio on a pixel-by-pixel basis.

The success of this DI depends on two factors: (1) the disturbance must generate a large enough signal to detect and (2) the signal must be greater than the natural variability. Because 2003 was the first full year of data collected by the Aqua/MODIS sensor, a multiyear mean-maximum LST/EVI ratio was not possible at the time of

study. However, as a longer data set becomes available, the multiyear mean-maximum value computed at each pixel will better represent the undisturbed energy balance of the land surface and provide a solid baseline to assess departure from the range of natural variability.

The logic behind Eq. 1 is illustrated in the conceptual DI model (Fig. 2). If a given pixel is not disturbed, the DI will be near unity (e.g., multiyear mean equals 1.0). However, the energy balance of a land area is not static and will vary within a range of natural variability (shown in green). Fluctuations within the range of natural variability occur during both dry and wet years. When a major disturbance event, such as wildfire occurs, LST will increase and EVI will decrease the following year, resulting in a value that is significantly larger than the multiyear mean. The disturbance event (shown in red) is detected as the signal moves outside the range of natural variability. As the area recovers from disturbance, as defined by increasing EVI and decreasing LST, the bidirectional nature of the DI will track the incremental change toward recovery and the range of natural variability (Fig. 2). Annual grasslands are one exception, because of the potential for quick recovery and a higher postfire EVI the year following disturbance. The general concept that EVI decreases after the disturbance event is still the same, but the relative time scale of the recovery process is much quicker. In the case of irrigation, LST decreases and EVI increases, resulting in a decreased ratio relative to the multiyear pre-irrigation energy balance of the land area. Irrigation disturbance (shown in blue) will be detected as the signal again moves outside the range of natural variability.

The MODIS instrument and data

As part of the Earth Observing System, the first MODIS instrument on the Terra platform was launched on 18 December 1999 and the second MODIS instrument on the Aqua platform was launched on 4 May 2002. The strengths of the MODIS instruments are global coverage, high geolocation accuracy, high radiometric resolution, and accurate calibration in the visible, near-infrared and thermal infrared (TIR) bands (Wan et al. 2004). LST from the Aqua/MODIS sensor was chosen for this study because of Aqua's afternoon overpass time of approximately 13:30 hours. Compared to the Terra/MODIS sensor's overpass time of 10:30 hours, Aqua's afternoon overpass retrieves LSTs that are much closer to the maximum daily temperature of the land surface. Measurements close to the peak of diurnal fluctuation better reflect the thermal response of rising leaf temperatures due to decreased latent heat flux as stomata close, and soil litter surfaces dry, accentuating differences in LST among vegetation covers. As a result, it is more suitable for regional and global change studies (Wan et al. 2004).

Radiometric LST is one of the key parameters in the physics of land surface processes on regional and global scales, combining surface-atmosphere interactions and the energy fluxes between the atmosphere and the land

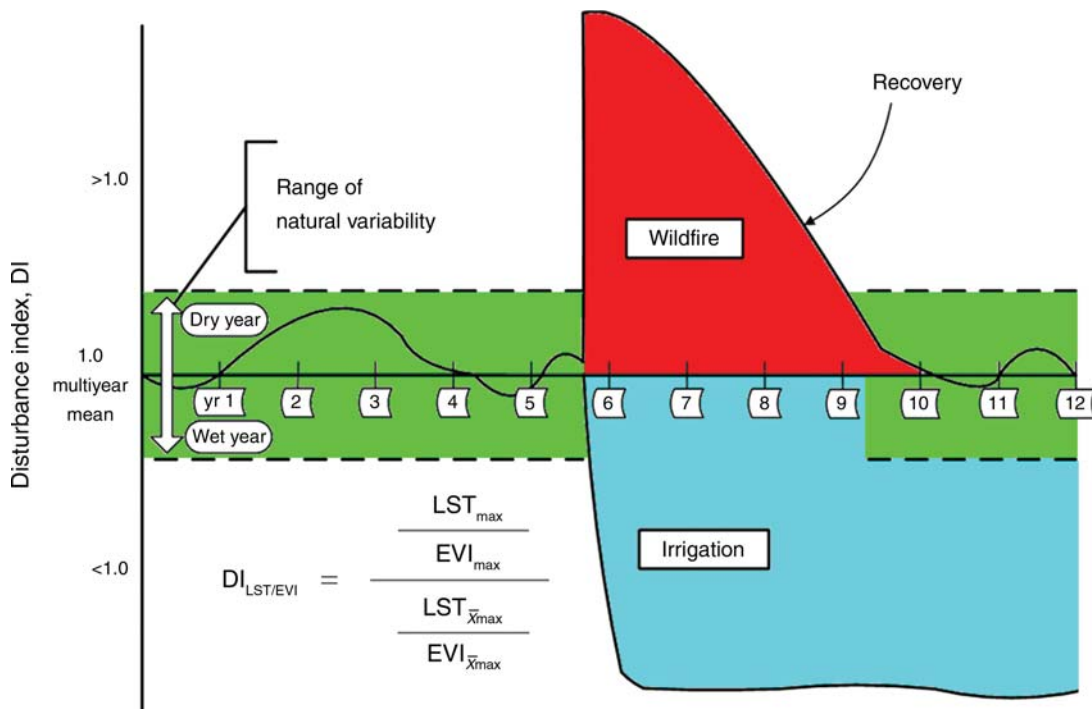


FIG. 2. The $DI_{LST/EVI}$ algorithm (where DI is the disturbance index, LST is the land surface temperature, and EVI is the Enhanced Vegetation Index) with a conceptual model illustrating the energy balance of a given land area through time. Under normal conditions, the current-year LST_{\max} and EVI_{\max} values will be similar to the multiple-year mean-maximum values, indicated by the multiyear mean of 1.0. Normal conditions exist within a range of natural variability that is defined by fluctuations between wet and dry years (green zone). Disturbance causes changes in the current-year LST_{\max} and/or EVI_{\max} values. In the case of wildfire, the LST_{\max} increases and the EVI_{\max} decreases, resulting in a larger current-year ratio relative to the multiyear mean and a divergence from the range of natural variability (red zone). If the LST_{\max} decreases and the EVI_{\max} increases from irrigation, the current-year ratio will become smaller than the multiyear mean, resulting in divergence from the range of natural variability (blue). The bidirectional aspect of the DI allows for the tracking of recovery as the maximum LST/EVI ratio returns toward the multiyear mean.

surface (Mannstein 1987, Sellers et al. 1988). It is defined as the radiation emitted by the top of the land surface as observed by MODIS at instantaneous viewing angles and can be described as "skin temperature." By comparison, standard air temperature measurements are taken 1.5 m above ground level with sensors protected from radiation and adequately ventilated. Because air is such a poor heat conductor, the LST in mid-summer can be 20°–30°C higher than the standard weather station temperature.

The LST of clear-sky pixels in MODIS scenes is retrieved from brightness temperatures in bands 31 and 32 with the generalized split-window algorithm (Wan and Dozier 1996). The MODIS LST bands based on TIR data are only available under clear-sky conditions because clouds inhibit satellite observations in the visible and TIR spectral ranges. The increase in quantity and the improvement in quality of the emissivity and temperature science data over the global land due to the increased number of MODIS observations in clear-sky conditions is a major advantage of the Aqua/MODIS data (Wan et al. 2004) and has resulted in a vastly improved LST product compared to the NOAA Advanced Very High

Resolution Radiometer (AVHRR) data that have been used to derive LST in previous studies.

The data set is composed of Aqua/MODIS eight-day composite daytime LST and Terra/MODIS 16-day composite EVI data for 2003–2004, and Terra/MODIS Land Cover Type 1 (IGBP) data. We used Terra/MODIS EVI because morning and afternoon overpass data sets can be interchangeably used for continental scale coverage (D. J. Mildrexler, *personal observation*) and the Terra EVI data was readily available in our data archives. All MODIS data used for this study are the most recently processed Collection 4 data with a spatial resolution of 1 km. MODIS quality control flags were used for the LST and EVI data. The Hierarchical Data Format-Earth Observation System (HDF-EOS) data were then converted to raster images for further analysis.

Testing the disturbance index

Keeping in mind that the DI is designed for global implementation, we tested the algorithm in the western United States, extending from the Pacific Coast to east of the Rocky Mountains (Fig. 3). The study domain encompasses one of the strongest hydrologic gradients

in the country and a broad range of bioclimatic regions, including the Pacific Northwest rain forests, the Great Basin, the Intermountain region, the High Plains, and the southwestern deserts.

Relationship between land cover stratified mean-maximum LST and EVI

To evaluate the biophysical relationship between maximum LST and maximum EVI across the study area in the LST–VI space, we calculated the land cover stratified mean-maximum LST and EVI. The MODIS land cover was used to assign pixels to a land cover type. This provided a consistent grouping method and the means to explore land cover stratified energy balance relationships in the LST–VI space across the western United States. Computation of the mean-maximum LST and EVI for each land cover class included every pixel in the study domain (excluding water and snow/ice). The mean-maximum LST was calculated as the sum of the highest temperature at each pixel during an annual period within a given land cover type divided by the number of pixels within that land cover type. The mean-maximum EVI was computed in a similar manner. The land cover stratified mean-maximum LST and the mean-maximum EVI data were tested for normality. To test the significance of the relationship between EVI and LST at the continental scale, Pearson's correlation analysis (r) was used, and the confidence limits (CL) surrounding r were calculated (Zar 1996).

Comparison of DI to wildfire perimeter maps

Wildfire often results in an abrupt, clearly defined boundary between the disturbed and undisturbed portions of the landscape and provides a negative disturbance (i.e., reduces vegetation cover) with independently confirmed, well-documented data sets for verification. We verified the DI results based on the demonstration of close association with fire perimeter maps from the Northern Rockies Coordination Group (*available online*)³ and the United States Forest Service. Fire perimeters were obtained by interpretation of infrared imagery, aerial and field-based Global Positioning System surveys, and on screen digitization. While fire perimeter maps do provide a high resolution data set for evaluating the periphery of fires, they do not differentiate between unburned and burned areas within the fire perimeter. Fire perimeter maps for the 2003 fire season include numerous fires in the Northern Rockies of Montana, the Needles and Fawn Peak Fires in the North Cascades of Washington, the Booth and Bear (B and B) Fire in the central Cascades of Oregon, and several fires in the Coast Ranges of California. We also compared DI results to the 2003 1-km resolution MODIS active fire detections data (Giglio et al. 2003). The MODIS fire detections data are a *daily* product that

identifies active fires at the time of satellite overpass, requiring sophisticated masking techniques to avoid excessive false alarms and provide real-time information that is necessary for fire management purposes. The MODIS active fire detections are discerned using the 1-km thermal bands of MODIS, and detections are provided as the centroids of the 1-km pixels.

Additionally, the DI was designed to detect changes in vegetation cover associated with recovery of disturbed areas. Wildfires from 2002 occurred prior to the Aqua/MODIS LST data used for this study and provide an opportunity to evaluate recovery from 2003 through 2004. Recovery was verified using fire perimeter maps from 2002, including the Biscuit Fire in southwest Oregon, the Rodeo Chediski Fire in east-central Arizona, and the 2002 MODIS active fire detections data.

DI response to irrigated plantation

As an example of positive disturbance, we examined one of the most heavily irrigated crops in the Columbia River Basin (*Populus* spp. tree farm) and the directly adjacent area of semiarid natural vegetation in eastern Oregon's high desert. By examining the maximum LST and EVI values over such a contrasting scene, we can begin to understand the response of the LST/EVI ratio to irrigation. The location of the poplar tree farm (45.8° N, 119.5° W) was confirmed with 15-m resolution ASTER imagery and identified with MODIS land cover classification data. Two five-pixel transects were established; one within the poplar tree farm, classified as deciduous broadleaf forest (DBF), and one within the adjacent native plant community, classified as a mixture of open shrublands (OS) and grasslands (G). We extracted the maximum LST and EVI value at each pixel along both transects. We then computed the average maximum LST and EVI for both transects. Finally, we computed the LST/EVI ratio and compared the difference between land covers.

DI response to climatic variability

Previous studies have shown that the response of vegetation to climatic variability can vary greatly across ecosystems and that annual herbaceous ecosystems (e.g., grasslands and croplands) display the greatest interannual variability in ANPP under natural precipitation patterns (Knapp and Smith 2001). White et al. (2005) used 13 years of NDVI data to examine the interannual vegetation variability over the continental United States and identified the High Plains, the Snake River Plain, and the Columbia Plateau in the western United States as areas of high vegetation variability. To explore the response of the DI to climate variability, we used precipitation anomaly maps for 2003 and 2004 from the Spatial Climate Analysis Service Prism data collection (*available online*).⁴ Precipitation anomaly maps show

³ <http://www.fs.fed.us/r1/firegis/2003web/dataindex.htm>

⁴ <http://www.ocs.oregonstate.edu/index.html>

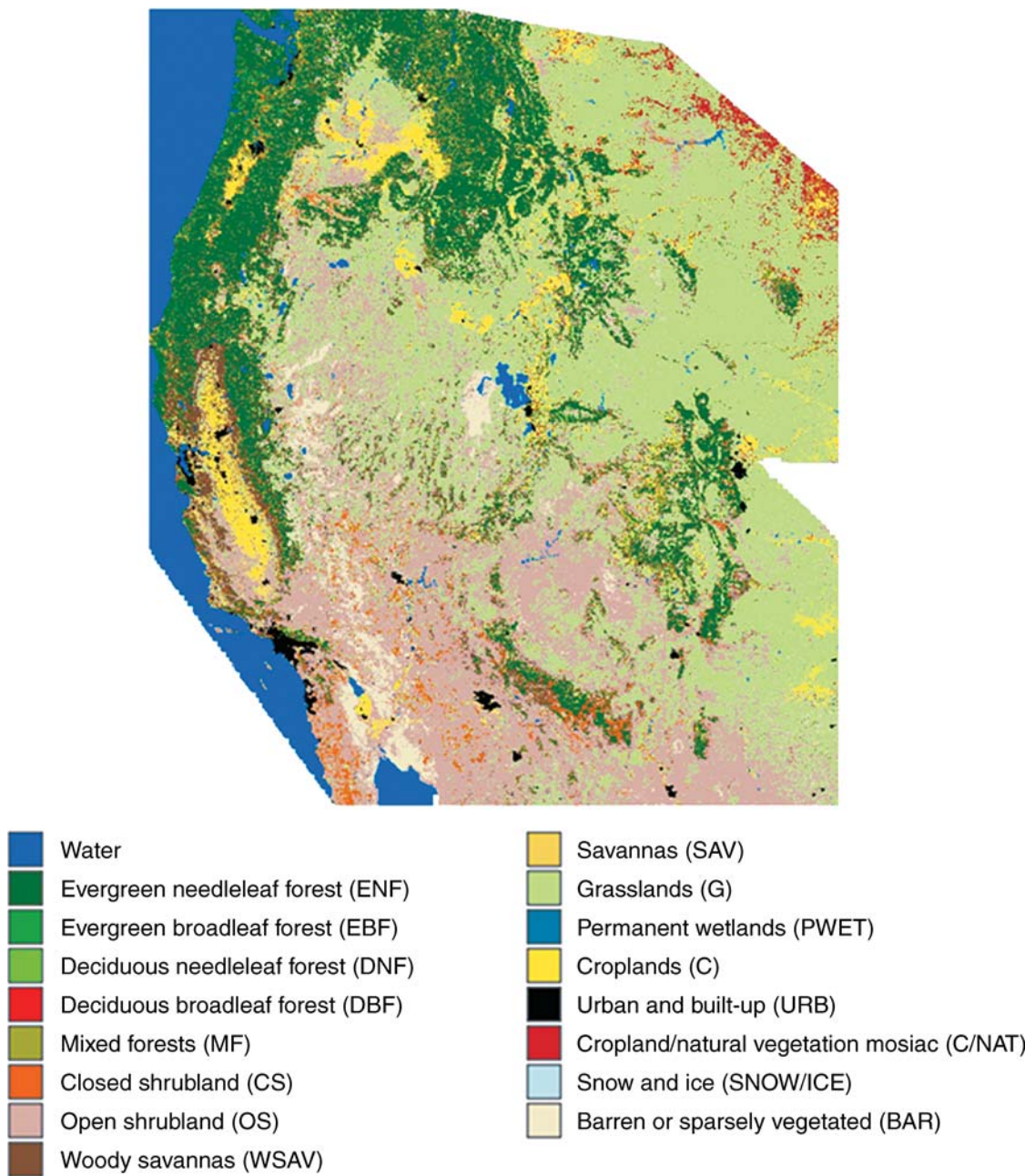


FIG. 3. Testing the DI across the western United States, a study domain that encompasses a broad range of bioclimatic regions and contains one of the strongest hydrologic gradients in North America (MODIS tiles h08v04, h08v05, h09v04, h09v05, and h10v04). Land cover classes are from the Terra/MODIS Land Cover Type 1 (IGBP).

precipitation as a percentage of the normal precipitation between 1971 and 2000 at a 4-km resolution.

RESULTS

Basic biophysical relationship between mean-maximum LST and EVI

The land cover class stratified mean-maximum EVI and mean-maximum LST over the western United

States for 2003 through 2004 were strongly negatively correlated ($r = -0.81 \pm 0.23$; Fig. 4) with 95% confidence ($P \leq 0.001$). The land cover stratified grouping of the mean-maximum LST and EVI in the LST–VI space was similar to the groups hypothesized by Nemani and Running (1997: Fig. 1). Water-limited biomes (barren, shrublands) occupy the high-LST/low-EVI area of the LST–VI space. Land cover classes characterized by annual herbaceous vegetation (grasslands, savanna, and

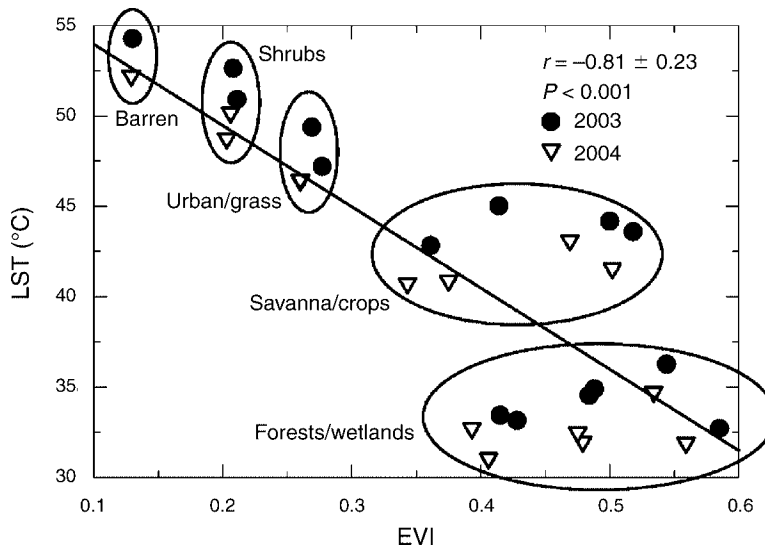


FIG. 4. Every 1-km pixel, excluding water and snow/ice, within the western United States study domain was included within the land cover stratified mean-maximum values displayed in the LST–EVI space. The energy balance relationship and land cover grouping are similar to the disturbance trajectory and four simple groups conceptualized by Nemani and Running (1997; see Fig. 1). Correlation is given with 95% CI.

croplands) occupy the center of the LST–VI space. Atmospherically coupled land covers (forests, wetlands) occupy the low-LST/high-EVI area of the LST–VI space. A summary of land cover stratified mean-maximum LST and EVI values and their standard deviation is given in Table 1.

Application of the DI algorithm

We applied the DI algorithm to the MODIS data for the years 2003 and 2004 across the western United States. The mean DI value for the entire study area (0.99) with all pixels combined was rounded to 1.0. The DI scale extended from 0.2 to 4.0. The range of natural variability was defined as the values that were within one standard deviation (± 0.32) of the mean (1.0). Any values within the range of natural variability (0.68–1.32) were mapped

as no color. Values >1.32 (mapped in orange) and 1.64 (mapped in red) indicate that the DI results were one or more standard deviations above the mean and coincide with disturbances such as wildfire scars and precipitation deficit anomalies. Values <0.68 (mapped in light blue) and 0.36 (mapped in dark blue) indicate that the DI results were one or more standard deviations below the mean value and coincide with recovery of disturbed landscapes or precipitation surplus anomalies.

Wildfire detection: DI > 1.0

Fire is the prominent disturbance event in the western United States, and large wildfires occurred throughout the study area in 2003. We examined the correspondence between the DI and case examples where precise knowledge of the spatial extent of wildfires is well

TABLE 1. Biome stratified mean-maximum Enhanced Vegetation Index (EVI) and mean-maximum land surface temperature (LST) with standard deviations in parentheses for 2003 and 2004.

Land cover	2003		2004	
	EVI _{max} (SD)	LST _{max} (SD)	EVI _{max} (SD)	LST _{max} (SD)
ENF	0.42 (0.12)	33.4 (5.5)	0.41 (0.11)	31.1 (5.3)
EBF	0.59 (0.14)	32.7 (6.1)	0.56 (0.13)	31.9 (5.2)
DNF	0.49 (0.08)	34.9 (4.3)	0.48 (0.08)	32.0 (4.3)
DBF	0.54 (0.11)	36.3 (5.7)	0.53 (0.11)	34.7 (5.7)
MF	0.48 (0.11)	34.6 (5.4)	0.48 (0.11)	32.5 (5.0)
CS	0.21 (0.09)	50.9 (6.9)	0.20 (0.08)	48.8 (6.8)
OS	0.21 (0.10)	52.6 (6.4)	0.21 (0.10)	50.2 (6.7)
WSAV	0.36 (0.12)	42.8 (6.7)	0.34 (0.11)	40.7 (6.0)
SAV	0.50 (0.12)	44.2 (7.4)	0.47 (0.12)	43.1 (7.9)
G	0.27 (0.11)	49.4 (5.6)	0.26 (0.11)	46.4 (5.9)
PWET	0.43 (0.18)	33.2 (9.4)	0.39 (0.19)	32.7 (8.8)
C	0.52 (0.13)	43.6 (4.8)	0.50 (0.13)	41.6 (5.5)
URB	0.28 (0.11)	47.2 (5.7)	0.26 (0.09)	46.5 (5.7)
C/NAT	0.41 (0.10)	45.0 (3.8)	0.38 (0.11)	40.9 (4.7)
BAR	0.13 (0.09)	54.3 (7.5)	0.13 (0.09)	52.2 (7.7)

Note: See Fig. 3 for explanations of all land cover abbreviations.

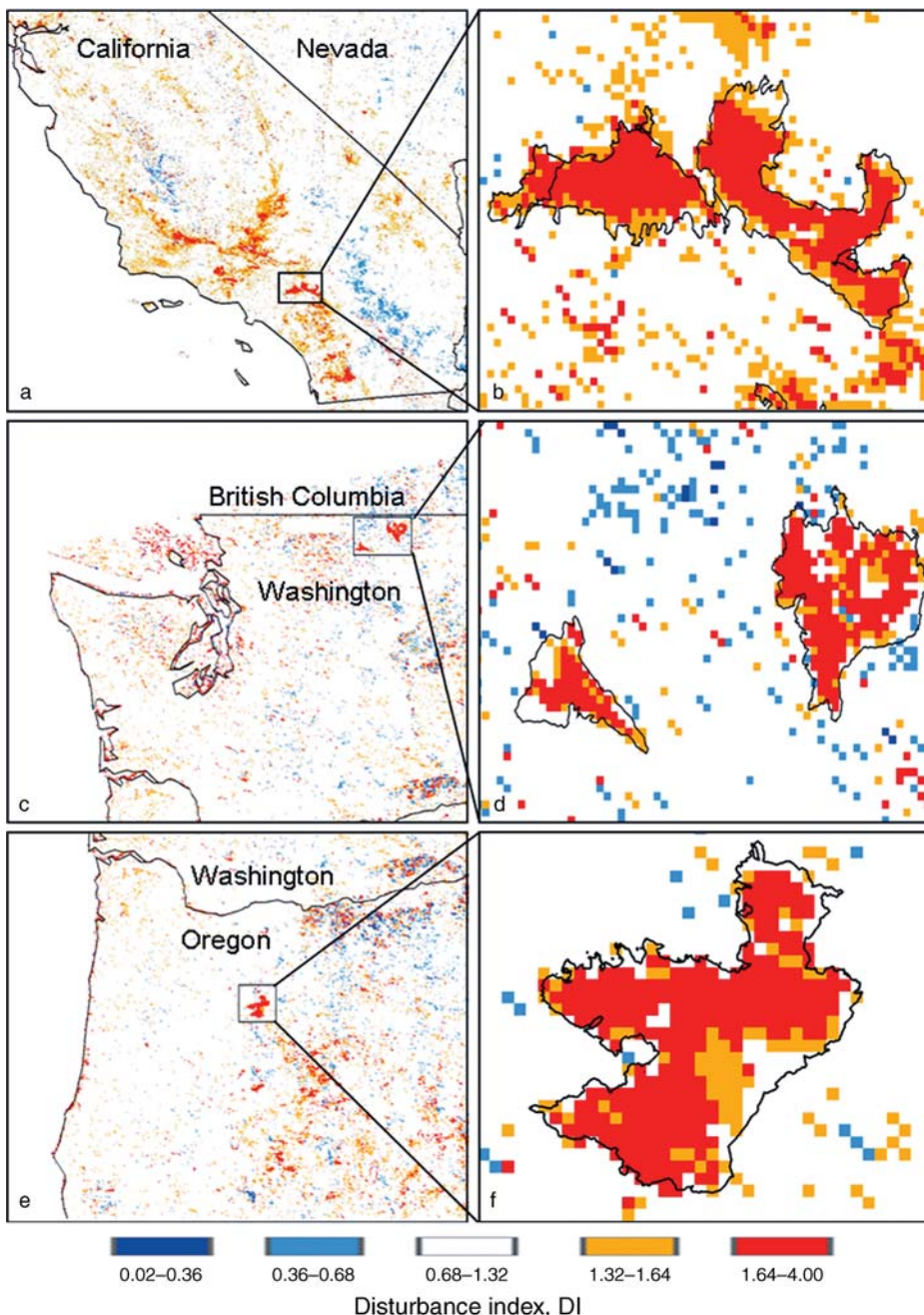


FIG. 5. Wildfire detection results showing a detailed comparison with independently confirmed, well-documented fire perimeter maps (black outlines) for the (a, b) 2003 southern California fires, (c, d) Washington's Fawn Peak and Needles Fires, and (e, f) Oregon's B and B Complex Fires. These fire perimeters were obtained by interpretation of infrared imagery, aerial and field-based Global Positioning System surveys, and on-screen digitization. High values detected by the disturbance index ($DI > 1.64$) indicate a large divergence from the range of natural variability.

known. The spatial association between the high values (>1.64) detected by the algorithm and the fire perimeter maps (black outlines) are shown in Fig. 5. The DI clearly detects disturbance that shows close correspondence with the fire perimeter maps for the Padua, Grand Prix, and Old Fires in southern California (Fig. 5a, b), the Needles and Fawn Peak Fires in Washington (Fig.

5c, d), and the B and B Fire in Oregon (Fig. 5e, f). Note that the fire perimeter maps for the Needles and Fawn Peak Fires (Fig. 5d) and the B and B Fire (Fig. 5f) cover a slightly larger surface area than the DI. Fire perimeter maps often overestimate total burned area because they include unburned “islands” within the fire perimeter as burned. The DI is based on pure radiometry and could

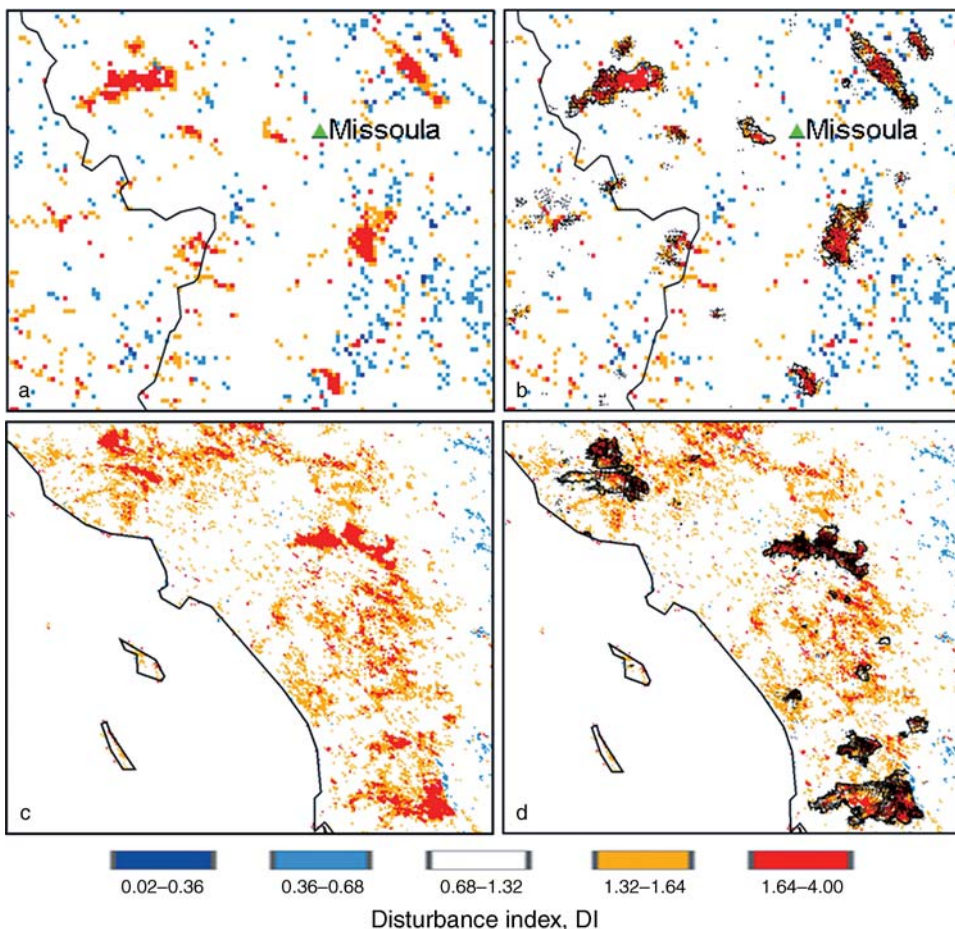


FIG. 6. Correspondence between the DI results, the MODIS active fire-detection data (black dots) and fire perimeter maps (black outlines) for (a, b) the 2003 wildfires near Missoula, Montana, and (c, d) the 2003 southern California wildfires. The southern California fires occurred in savanna and shrublands, vegetation types with the highest frequency of major disturbance at the global scale. The maximum LST increased in the fire areas in 2004, and the DI detected the increase relative to 2003.

provide more accurate information on the spatial extent and severity of wildfire.

The MODIS fire detection data and fire perimeter maps were used together to evaluate the DI results across a larger area. Numerous wildfires burned around Missoula, Montana, during the 2003 wildfire season. The high values (>1.64) detected by the algorithm show close correspondence with the 2003 fire perimeter maps and MODIS fire detection data (Fig. 6b, black dots). The 2003 southern California fires provided a good opportunity to assess the DI results in a mixed land cover area, including savanna and shrublands, two of the land covers with the highest frequency of major disturbance on the global scale (Potter et al. 2003). The 2004 maximum LST increased in the areas disturbed by the 2003 wildfires (data not shown), and the DI clearly distinguished these areas from the surrounding landscape (Fig. 6c). The high values (>1.64) detected by the DI are tightly coupled with fire perimeter maps and the MODIS fire detection for the 2003 California wildfires (Fig. 6d). However, there are areas within the fire

perimeter maps that the DI detects as disturbance and the MODIS active fire detections data does not. Further research should be done using case examples where precise knowledge of the spatial extent, severity, and unburned areas within the fire perimeter are known to determine if the DI is detecting disturbance that the MODIS active fire detections is missing.

Disturbance recovery detection

Tracking recovery of disturbed areas is important for understanding how much of the land surface is in a state of recovery at any one time, how long recovery takes, and if recovery to the pre-disturbance range of natural variability is occurring. The Biscuit and Rodeo Chediski Fires of 2002 occurred primarily in evergreen needleleaf forest (ENF) and prior to the first full year of Aqua/MODIS data collection (2003). With only two years of data defining the range of natural variability, we calculated the ENF land cover class stratified DI standard deviation (0.24) to more accurately represent the range of natural variability for ENF. The DI

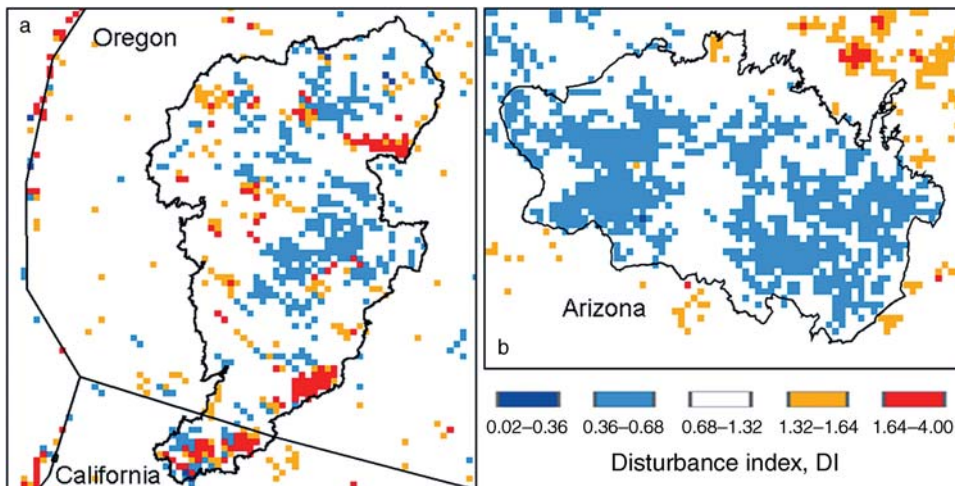


FIG. 7. Fire perimeter maps for (a) the Biscuit and (b) Rodeo Chediski Fires of 2002. After one year of recovery, the low DI values (<0.76) over large portions of the fire areas illustrate the change in the LST/EVI ratios resulting from revegetation from 2003 to 2004. The wildfires occurred prior to the data used for this study, but recovery is an incremental process and will continue until the LST/EVI ratio returns to the range of natural variability.

detected recovery from 2003 to 2004 illustrated by the low values (<0.76) that correspond with fire perimeter maps for the Biscuit and Rodeo Chediski Fires (Fig. 7a, b). The lowering of the 2004 LST/EVI ratio due to the increase in EVI_{max} and decrease in LST_{max} relative to 2003 is strong evidence that revegetation of burned areas is identified by the DI. Recovery is found coinciding with the 2002 MODIS fire detection data throughout the western United States.

Detection of irrigated plantations: $DI < 1.0$

Just as wildfire provides a negative disturbance that causes abrupt temporal and spatial changes to vegetation structure and surface energy partitioning, irrigation in semiarid and arid environments provides a clearly defined positive disturbance to evaluate. The poplar tree farm, located within the continental interior semiarid climate of northeast Oregon, is classified as deciduous broadleaf forest (DBF) by the MODIS land cover (Fig. 8a). The MODIS EVI product clearly shows the dense vegetation of the poplar farm study area ($EVI = 0.66-0.99$; Fig. 8b) relative to the adjacent OS and G covers ($EVI = 0.15-0.32$).

The poplar tree farm can be seen in the lower left of the 15-m resolution ASTER image as dark red blocks that sharply contrast with the surrounding landscape (Fig. 8c). The Columbia River bisects the top of the image and various agricultural lands, as well as undeveloped areas, surround the heavily irrigated tree plantation. The maximum LST of the poplar tree farm for 2003 and 2004 is 33.0°C and 36.0°C , respectively, and is significantly different from the adjacent mixed OS and G transect (60.4°C and 59.4°C , respectively) with 97% confidence ($P \leq 0.001$). The nearly 30°C difference in maximum LST between these adjacent land cover types highlights the influence of vegetation cover on LST.

Furthermore, the 2003 LST/EVI ratio for the semiarid area is ~ 250 , more than six times greater than the poplar tree farm LST/EVI ratio (40). This illustrates the dramatic impact that irrigation can have on a landscape and the resulting LST/EVI signal.

Test of DI for the western United States

Based on only two years of data (2003 through 2004), the continuous DI results for the western United States study area are shown in Fig. 9. Anomalous patterns emerge, especially over the High Plains region, the Columbia River Plateau, and in parts of the southwestern United States. As discussed earlier, accurately distinguishing disturbance from natural variability is the most difficult challenge in developing a disturbance index. Interannual precipitation variability is one of the most common forms of natural variability, and we assessed the impact of precipitation anomalies during 2003 and 2004 on the DI results. As additional years of data become available, the zone of natural variability will be more accurately defined, and we can further investigate the persistence of these anomalies. If conditions persist, the impact of weather variability on the DI could mark the onset of non-instantaneous disturbance events, such as drought.

Climate variability analysis: the High Plains

The DI results for the northern High Plains show high values extending throughout southeastern Montana, northeastern Wyoming, southwestern North Dakota, and western South Dakota (shown in orange and red in Fig. 10a). This area is dominated by grasslands and croplands, land cover types with high sensitivity to interannual precipitation. Precipitation anomaly maps for the same area show average precipitation in 2003 (Fig. 10b) followed by a widespread decrease to 51–70%

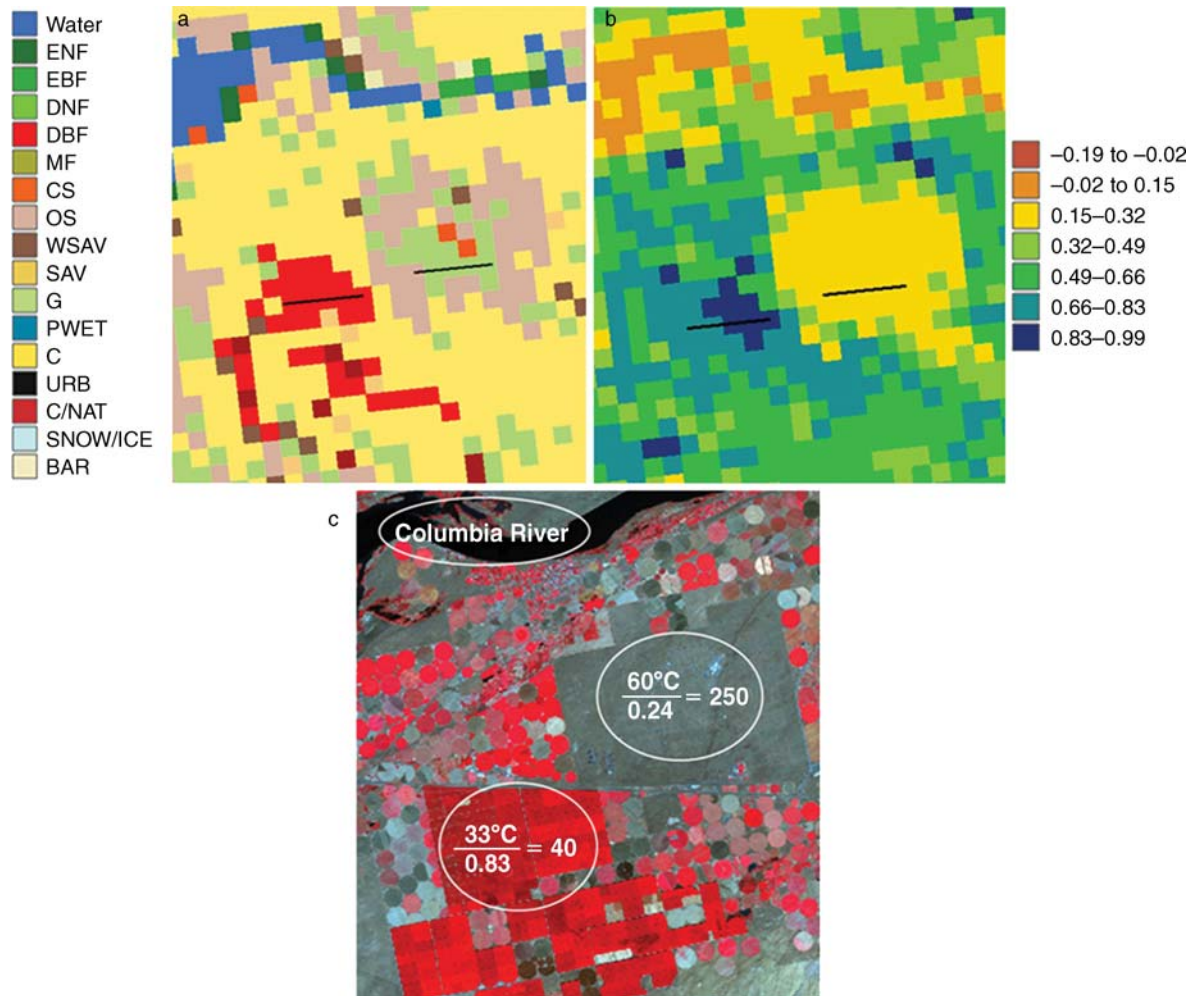


FIG. 8. (a) A heavily irrigated poplar tree farm in northeast Oregon, classified as deciduous broadleaf forest (in red) by the MODIS Land Cover image, grows immediately adjacent to the natural semiarid vegetation, classified as open shrubland and grassland. (b) Maximum LST and EVI values were extracted along two transects (shown in black) and the LST/EVI ratios compared. See Fig. 3 for explanations of land cover abbreviations. (c) The ASTER image (15 m) shows the sharp contrast between the poplar tree farm (lower left, dark red squares) and the neighboring natural vegetation (upper right, gray area). As indicated by the large difference in the LST/EVI ratios, initiation or stopping of irrigation in a semiarid landscape would be clearly detected by the DI.

and 71–90% of normal precipitation in 2004 (Fig. 10c). In response to the precipitation deficit, the EVI_{\max} values decreased in 2004 relative to 2003. This increased the 2004 LST/EVI ratio relative to 2003, and resulted in DI values greater than one.

Results for the southern High Plains show a large area with low DI values extending throughout much of New Mexico, southern Colorado, and western Texas (mapped in blue in Fig. 10d). This area has values greater than one standard deviation below the mean, indicating that the 2004 LST/EVI ratio was less than the 2003 LST/EVI ratio. Precipitation anomaly maps show widespread deficit (31–50% and 51–70% of normal) in the southern High Plains region during 2003 (Fig. 10e), followed by 171–200% of normal precipitation in 2004 (Fig. 10f). The temporal and spatial correspondence

between a large precipitation surplus anomaly and a significant increase in ANPP in grasslands is strong evidence that the DI is responding to interannual rainfall in this area.

DISCUSSION

We have described in detail a new algorithm for global, automated disturbance detection using MODIS 1-km LST and EVI data and examined the results at multiple scales. The annual changes in the maximum LST/EVI ratios closely correspond to wildfire perimeter maps across the study area (Fig. 5), highlighting the potential for the DI to provide detailed, accurate information on the location and spatial extent of wildfire. At the regional scale, the strong correspondence between MODIS fire detection data and disturbance

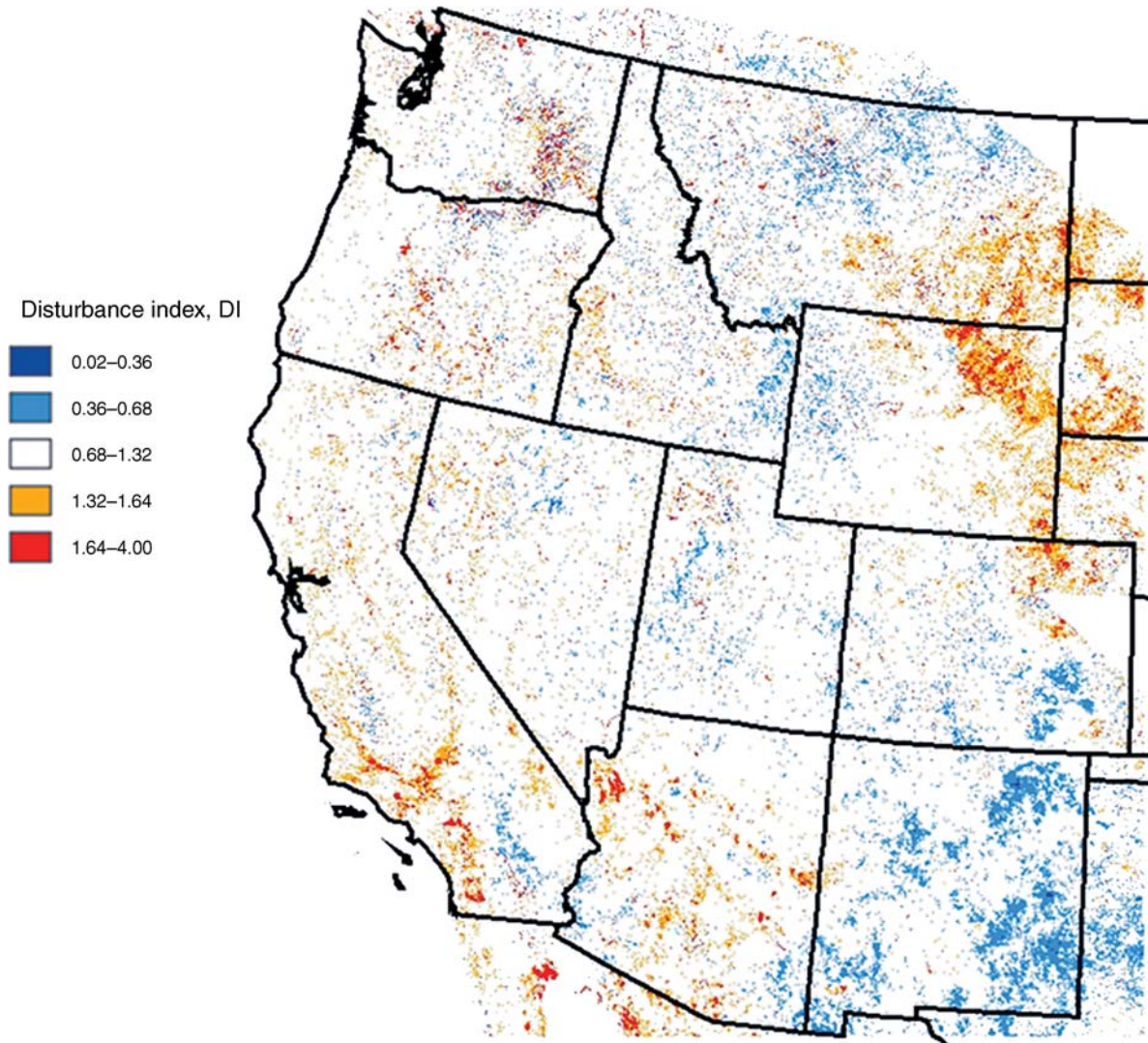


FIG. 9. With only two years of data (2003 through 2004), we present the continuous DI results for the western United States using 1.0 standard deviation (0.32) from the mean (1.0) to define the range of natural variability. In addition to high values associated with wildfire (see Fig. 5) and recovery (see Fig. 7), large areas are detected as disturbed in the High Plains and in the Columbia River Plateau. We did not consider interannual variability an ecological disturbance; additional years of MODIS data will help this automated algorithm separate normal variability from disturbance in annual herbaceous ecosystems.

detected by the DI illustrates the potential of the DI to detect disturbance over large spatial areas (Fig. 6). The continuous DI results across the western United States study domain showed anomalous values in annual herbaceous ecosystems (e.g., High Plains, Columbia River Plateau) driven by variability in ANPP in response to precipitation anomalies (Fig. 10). For land covers with large interannual variability in ANPP (e.g., grasslands, croplands), two years of data is insufficient for defining the range of natural variability because fluctuations that would eventually fall within the range of natural variability with a longer data set are incorrectly detected as disturbed. We are optimistic that, with additional years of data, the range of natural variability for annual herbaceous ecosystems will be

redefined to incorporate this interannual variability and avoid false disturbance detections. For example, with five years of data, the current year ratios of maximum LST to EVI will be evaluated against four-year averages that will be computed on a pixel by pixel basis. Interannual variability over the four-year period will define a given pixels range of natural variability, and whether an event is detected as disturbance.

The strong negative correlation found between the mean-maximum LST and the mean-maximum EVI across the western United States from 2003 through 2004 (Fig. 4) supports the principle that surface temperature decreases with an increase in vegetation density through transfer of energy to latent heat. The strength of this relation found at the continental scale in

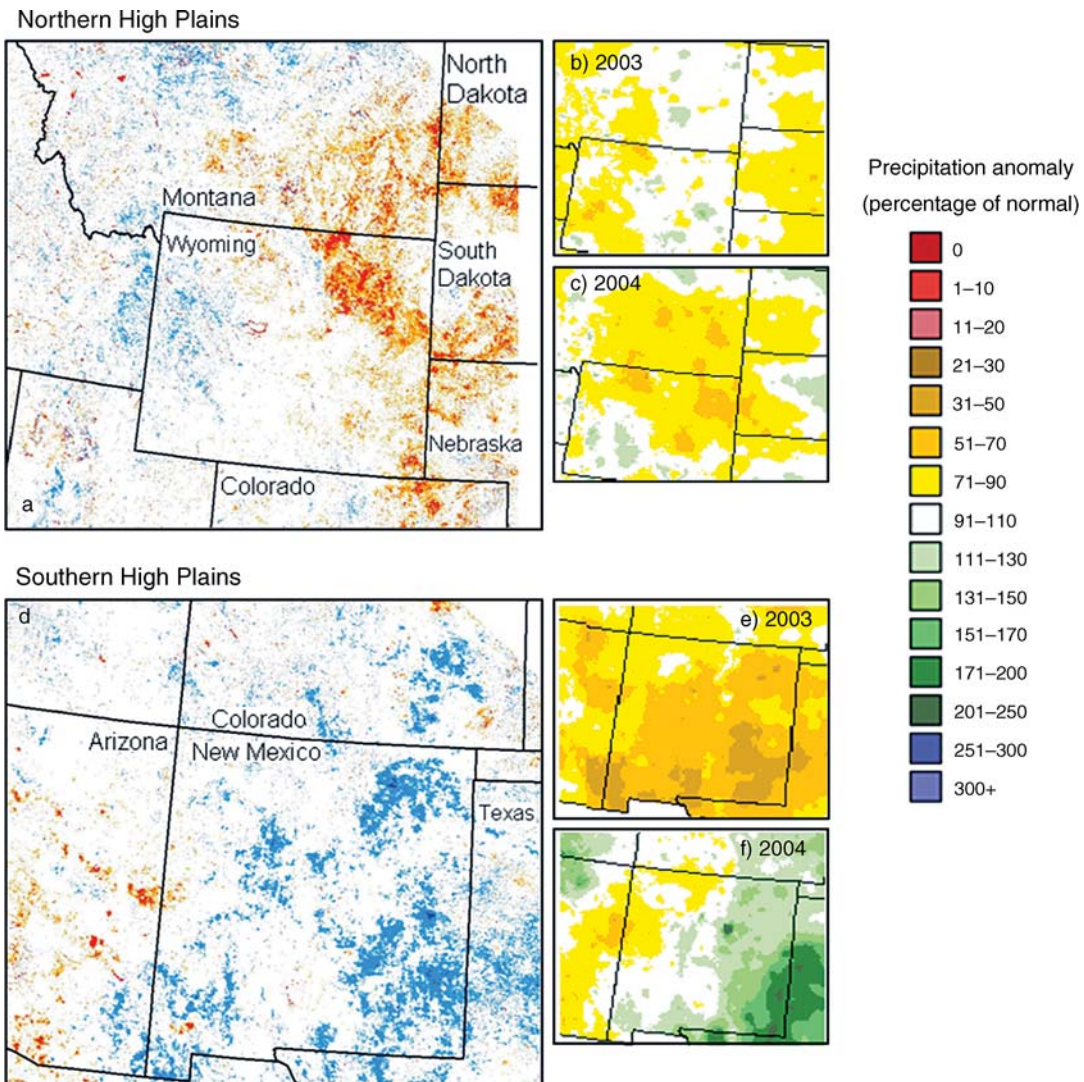


FIG. 10. The High Plains region is composed of grasslands, croplands, and open shrublands, annual herbaceous ecosystems that display high interannual variability in annual net primary productivity (ANPP) in response to precipitation variability. (a) In the northern High Plains, anomalously high DI values (in orange and red) extend over a large area. (b, c) Precipitation anomaly maps show that the same area received normal precipitation levels in 2003 (b), followed by 51–70% and 71–90% of normal precipitation over large areas in 2004 (c). (d) The southern High Plains region shows low DI values (in light and dark blue) that extend over a large area. (e, f) Precipitation in this area was 31–70% of normal in 2003 (e), followed by 151–200% of normal in 2004 (f). Maps copyright © 2004 and 2005, PRISM Group, Oregon State University (<http://ocs.oregonstate.edu/prism>). Panels a, b, and c were created 2 Aug 2004; panels d, e, and f were created 11 May 2005.

a bioclimatically diverse area suggests that the DI is founded on universal principles. This robust and consistent radiometric relationship will be revisited for each individual pixel at the global scale every year. The power of this approach is that, over time, each pixel is self-normalized, defining its own range of natural variability. Monitoring at the global scale will be economical and simple because the DI is computationally inexpensive and highly repeatable.

Over a three-year period, evidence of revegetation of burned areas can be clearly identified and mapped (Fig. 7). This result suggests that the DI algorithm is sensitive

to the incremental annual changes associated with the return of the annual maximum LST/EVI ratio to the range of natural variability. Biomes have different strategies for recovery, and, thus, the rate of recovery of different ecosystems varies. For example, following wildfire, certain chaparral species can recover quickly by re-sprouting from carbohydrate-rich root burls, whereas pine forests regenerate more slowly and from seed. The length of time for a pixel to return to the range of natural variability defines the length of recovery. In a rapidly changing world, tracking recovery over the earth surface could aid in understanding the natural differ-

ences that occur within similar and contrasting ecosystems on a global basis.

The positive disturbance analysis illustrates that both variables in the DI algorithm respond to the biophysical impacts of irrigation (Fig. 8c). Even if pre-disturbance information on a given irrigated area is not available, if irrigation ceases or changes significantly, the DI will detect the change in energy exchange dynamics and vegetation density and redefine the range of natural variability and disturbance for that area. Tracking changes in irrigated lands globally could provide valuable information as demand for freshwater resources continues to grow, with concomitant implications for food scarcity.

CONCLUSIONS

We have described and tested a computationally efficient, automated algorithm for systematic global disturbance detection. It is based on annual maximum composite Aqua/MODIS LST and Terra/MODIS EVI data that avoids the high natural variability associated with tracking LST over short temporal periods. In future implementations of this DI algorithm, we suggest use of the Aqua sensor for both LST and EVI for simplicity of processing. The DI is based on two sound fundamental principles: (1) that vegetation, when left undisturbed, will achieve maximum coverage for a specified environment, and (2) that disturbance of vegetation will result in a significantly different surface coverage and a commensurate change in the maximum surface temperature. The maximum LST/EVI ratio takes into account both the potentially most vulnerable biotic (vegetation) and abiotic (LST) components of the terrestrial ecosystem to disturbance.

The ability of the DI to accurately detect the location and spatial extent of disturbance across broad scales and over various biomes as seen in this study suggests that the DI could serve as a “first-look” disturbance detection algorithm at the global scale. Information on the location and spatial extent of disturbance events and recovery globally could help to reduce some of the uncertainty in understanding the contribution of these events to the global carbon cycle.

A limitation of the annual maximum compositing methodology of the DI algorithm was found in annual herbaceous ecosystems with the potential for very rapid rates of post-disturbance recovery. These ecosystems regularly have a higher postfire EVI the year following disturbance. The DI concept of EVI decreasing after disturbance would work right after the disturbance event, suggesting the need for a shorter time composite. A seasonal calculation may need to be incorporated into the algorithm for annual herbaceous dominated land covers.

The DI will continue to refine the range of natural variability with each additional year of data. This will provide a solid basis from which to assess departure of disturbance events from, and recovery of ecosystems to, the normal condition. Disturbance detection in ecosys-

tems with high interannual variability will be significantly improved. The next step is to implement this methodology globally and explore the changes in the range of natural variability over a multiyear data set.

ACKNOWLEDGMENTS

This project would not have been possible without the financial support from the National Aeronautics and Space Administration (NASA) Earth Observing System (EOS) Natural Resource/Education Training Center (Grant Number NAG5-12540). The authors are grateful to R. Nemani for providing the foundation for this research, and Dorothy Thomas, Kerri Mich, and Jack Rainford of the United States Forest Service for providing fire perimeter maps for this study.

LITERATURE CITED

- Amiro, B. D., J. B. Todd, B. M. Wotton, K. A. Logan, M. D. Flannigan, B. J. Stocks, J. A. Mason, D. L. Martell, and K. G. Hirsch. 2001. Direct carbon emissions from Canadian forest fires, 1959–1999. *Canadian Journal of Forest Research* 31:512–525.
- Borak, J. S., E. F. Lambin, and A. H. Strahler. 2000. The use of temporal metrics for land cover change detection at coarse spatial scales. *International Journal of Remote Sensing* 21: 1415–1432.
- Canadell, J. G., et al. 2000. Carbon metabolism of the terrestrial biosphere: a multi-technique approach for improving understanding. *Ecosystems* 3:115–130.
- Carlson, T. N., F. E. Boland, J. K. Dodd, and S. G. Benjamin. 1981. Satellite estimation of the surface energy balance, moisture availability and thermal inertia. *Journal of Applied Meteorology* 20:67–87.
- Carlson, T. N., E. M. Perry, and T. J. Schmugge. 1990. Remote estimation of soil moisture availability and fractional vegetation cover over patchy vegetation. *Agricultural and Forest Meteorology* 52:44–60.
- Dale, V. H., S. Brown, R. A. Haeuber, N. T. Hobbs, N. Huntly, R. J. Naiman, W. E. Riebsame, M. G. Turner, and T. J. Valone. 2000. Ecological principles and guidelines for managing the use of land. *Ecological Applications* 10:639–670.
- Friedl, M. A., and F. W. Davis. 1994. Sources of variation in radiometric surface temperature over a tallgrass prairie. *Remote Sensing of Environment* 48:1–17.
- Giglio, L., J. Descloitres, C. O. Justice, and Y. J. Kaufman. 2003. An enhanced contextual fire detection algorithm for MODIS. *Remote Sensing of Environment* 87:273–282.
- Goetz, S. J. 1997. Multi-sensor analysis of NDVI, surface temperature and biophysical variables at a mixed grassland site. *International Journal of Remote Sensing* 18:71–94.
- Goward, S. N., G. D. Cruickshanks, and A. S. Hope. 1985. Observed relation between thermal emission and reflected spectral radiance of a complex vegetated landscape. *Remote Sensing of Environment* 18:137–146.
- Goward, S. N., and A. S. Hope. 1989. Evapotranspiration from combined reflected solar and emitted terrestrial radiation: preliminary FIFE results from AVHRR data. *Advanced Space Research* 9:239–249.
- Gurney, R., and P. J. Camillo. 1984. Modelling daily evapotranspiration using remotely sensed data. *Journal of Hydrology* 69:305–324.
- Holmgren, M., et al. 2006. Extreme climatic events shape arid and semiarid ecosystems. *Frontiers in Ecology and the Environment* 4:87–95.
- Hope, A. S., D. E. Petzold, S. N. Goward, and R. M. Ragan. 1986. Simulated relationships between spectral reflectance, thermal emissions and evapotranspiration of a soybean canopy. *Water Resources Bulletin* 22:1011–1019.
- Huete, A., K. Didan, T. Miura, E. P. Rodriguez, X. Gao, and L. G. Ferreira. 2002. Overview of the radiometric and

- biophysical performance of the MODIS vegetation indices. *Remote Sensing of Environment* 83:195–213.
- Huete, A., C. Justice, and W. v. Leeuwen. 1999. MODIS Vegetation Index (MOD 13) algorithm theoretical basis document. <http://modis.gsfc.nasa.gov/data/atbd/atbd_mod13.pdf>
- Huxman, T. E., et al. 2004. Convergence across biomes to a common rain-use efficiency. *Nature* 429:651–654.
- Knapp, A. K., and M. D. Smith. 2001. Variation among biomes in temporal dynamics of aboveground primary production. *Science* 291:481–484.
- Lambin, E. F., and D. Ehrlich. 1995. Combining vegetation indices and surface temperature for land-cover mapping at broad spatial scales. *International Journal of Remote Sensing* 16:573–579.
- Lambin, E. F., and D. Ehrlich. 1996. The surface temperature–vegetation index space for land cover and land-cover change analysis. *International Journal of Remote Sensing* 17:463–487.
- Mannstein, H. 1987. Surface energy budget, surface temperature and thermal inertia. Pages 391–410 in R. A. Vaughan and D. Reidel, editors. *Remote sensing applications in meteorology and climatology*. A Reidel Publishing, Dordrecht, The Netherlands.
- Nemani, R. R., L. L. Pierce, and S. W. Running. 1993. Developing satellite derived estimates of surface moisture status. *Journal of Applied Meteorology* 32:548–557.
- Nemani, R. R., and S. W. Running. 1989. Estimation of regional surface resistance to evapotranspiration from NDVI and thermal-IR AVHRR data. *Journal of Applied Meteorology* 28:276–284.
- Nemani, R. R., and S. W. Running. 1997. Land cover characterization using multitemporal red, near-IR, and thermal-IR data from NOAA/AVHRR. *Ecological Applications* 7:79–90.
- Pickett, S. T. A., S. C. Collins, and J. J. Armesto. 1987. Models, mechanisms, and pathways of succession. *Botanical Review* 53:335–371.
- Pickett, S. T. A., and P. S. White. 1985. The ecology of natural disturbance as patch dynamics. Academic Press, New York, New York, USA.
- Potter, C., P. Tan, M. Steinback, S. Klooster, V. Kumar, R. Myneni, and V. Genovese. 2003. Major disturbance events in terrestrial ecosystems detected using global satellite data sets. *Global Change Biology* 9:1005–1021.
- Price, J. C. 1990. Using the spatial context in satellite data to infer regional scale evapotranspiration. *IEEE Transactions on Geoscience and Remote Sensing* 28:940–948.
- Reice, S. R. 1994. Nonequilibrium determinants of biological community structure. *American Naturalist* 82:424–435.
- Roy, D. P., P. Kennedy, and S. Folving. 1997. Combination of the Normalized Difference Vegetation Index and surface temperature for regional scale European Forest cover mapping using AVHRR data. *International Journal of Remote Sensing* 18:1189–1195.
- Running, S. W., et al. 1994. Terrestrial remote sensing science and algorithms planned for EOS/MODIS. *International Journal of Remote Sensing* 15:3587–3620.
- Schimel, D. S., et al. 2001. Recent patterns and mechanisms of carbon exchange by terrestrial ecosystems. *Nature* 414:169–172.
- Sellers, P. J., F. G. Hall, G. Asrar, D. E. Strelzel, and R. E. Murphy. 1988. The first ISLSCP Field Experiment (FIFE). *Bulletin of the American Meteorological Society* 69:22–27.
- Sequin, B., and B. Itier. 1983. Using midday surface temperature to estimate daily evaporation from satellite thermal IR data. *International Journal of Remote Sensing* 4:371–383.
- Smith, R. C. G., and B. J. Choudhury. 1991. Analysis of normalized difference and surface temperature observations over southeastern Australia. *International Journal of Remote Sensing* 12:2021–2044.
- Sousa, W. P. 1984. The role of disturbance in natural communities. *Annual Review of Ecology and Systematics* 15:353–391.
- Tilman, D. 1985. The resource-ratio hypothesis of plant succession. *American Naturalist* 125:827–852.
- Turner, M. G., V. H. Dale, and E. E. Everham, III. 1997. Fires, hurricanes, and volcanoes: comparing large-scale disturbances. *BioScience* 47:758–768.
- van der Werf, G. R., J. T. Randerson, G. J. Collatz, L. Giglio, P. S. Kasibhatla, A. F. Arellano, Jr., S. C. Olsen, and E. S. Kasischke. 2004. Continental-scale partitioning of fire emissions during the 1997 to 2001 El Niño/La Niña Period. *Science* 303:73–76.
- Wan, Z., and J. Dozier. 1996. A generalized split-window algorithm for retrieving land-surface temperature from space. *IEEE Transactions on Geoscience and Remote Sensing* 34: 892–905.
- Wan, Z., Y. Zhang, Q. Zhang, and Z.-L. Li. 2004. Quality assessment and validation of the MODIS global land surface temperature. *International Journal of Remote Sensing* 25: 261–274.
- Waring, R. H., and S. W. Running. 1998. *Forest ecosystems: analysis at multiple scales*. Academic Press, San Diego, California, USA.
- White, A. B., K. Praveen, and D. Tcheng. 2005. A data mining approach for understanding topographic control on climate-induced inter-annual vegetation variability over the United States. *Remote Sensing of Environment* 98:1–20.
- Zar, J. H. 1996. *Biostatistical analysis*. Chapter 18. Prentice-Hall, New Jersey, USA.